2025 IEEE/SICE International Symposium on System Integration (SII)
January 21-24, 2025, Munich, Germany

# Implicit Extended Kalman Filter for Radar-Only 2D Odometry and Sensor-Vehicle Calibration

Titouan Tyack, Damien Vivet and Laurent Ferro-Famil

*Abstract*— **Accurate and robust pose estimation is essential for any autonomous vehicle. While sensors like GNSS, LiDAR, and camera are widely used for state estimation, they admit weaknesses under challenging environments e.g. poor satellite signals, low light, or adverse weather. Recent 3D and 4D radars have emerged as a robust alternative, providing sparse point clouds with information on the detected targets' range, angle, and radial velocity. As a result, interest in radar-based odometry (RO) has grown steadily. In this paper, we explore two aspects: radar-only ego-motion estimation and multi-radar-vehicle extrinsic calibration. We present a Doppler-based radar odometry algorithm using an Implicit Extended Kalman Filter and propose a novel, radar-only and target-less multi-radar-vehicle calibration method. An observability analysis is conducted to optimize sensor placement considering both the odometry and calibration. Finally, the proposed methods are validated through both simulation and real data.**

## I. Introduction

An accurate and robust pose estimation is a mandatory step for any autonomous vehicle. To solve this problem, Global Navigation Satellite System (GNSS), Inertial Measurement Unit (IMU), LiDAR or cameras are usually used individually or in combination to overcome their respective weaknesses. For instance, GNSS can be perturbed by the context of navigation due to non-line of sight satellites or multi-path errors [1]. Even if visual and lidar-odometry algorithms have shown excellent performances [2], [3] they also have strong limitations. Cameras are very sensitive to poor lighting conditions and both cameras and LiDARs are impacted by harsh weather conditions, such as heavy rain, snow or fog. To avoid such inconvenience the use of millimeter wave radar (mmW radar) sensors is becoming more and more significant. Indeed radar perception is almost insensitive to the aforementioned conditions. Moreover, such a sensor can measure both the range and direction of arrival but also the apparent radial velocities of the detected objects. For these reasons, radar-based odometry (RO) is more and more studied [4]. Radar Odometry has been first studied using rotating radars [5], we choose to focus on single-chip Multiple-Input Multiple Output (MIMO) radar sensors, as they are much cheaper and lighter. An additional solution to increase the odometry accuracy and robustness is the hybridisation with other sensors such as wheel odometry or Inertial Measurement Unit (IMU) composed of accelerometer, gyrometer (6-axis), and sometimes magnetometer (9-axis), barometer. However, when it comes to fuse data from different sensors, it is necessary to have an accurate estimate of all the extrinsic calibrations. Even if the calibration between cameras, LiDARs and IMU are well studied [6]–[8], the calibration between radar and other sensors is more and more needed.

In this paper, we propose to focus on both aspects. First, we are studying the possibilities of having a single or multi-radar-based odometry system for vehicle ego-motion. Then based on observability analysis and simulation we propose a solution for radar extrinsic calibration.

The main contributions of our paper are:

- An Implicit Extended Kalman Filter based radar-only ego-motion algorithm using Doppler measurements.
- A filter-based, target-less multi-radar extrinsic calibration algorithm.
- An observability analysis for both the egomotion and calibration parameters to evaluate the sensor placement.
- A validation of the proposed algorithms through both simulation and real data.

## II. Related Works

### A. Odometry

The studies presented here are mainly from the robotics community and thus use as an input data 3D or 4D pre-processed point clouds (scans), consisting of detected targets each carrying the information of range, angle and radial velocity. However, the presented techniques are also used in the radar community from raw data processed via Range, Doppler, Angle Fast Fourier Transform (FFT) to obtain the so-called radar data cube, and perform detection on it using a Constant False Rate (CFAR) Detector [9], [10].

We can divide radar odometry in two types : scan-matching-based approaches and direct single-scan estimation.

In the first type of approach, registration algorithms. In [11], a radar pose-graph SLAM using the classic ICP algorithm is presented. Zhang et al. [12] proposed a generalized-ICP (GICP) algorithm which uses plane-to-plane matching between radar keyframes. In [13] a 2D two-way weighted ICP algorithm is presented to estimate 2D pose. In [14], a Normal Distribution Transform (NDT) based scan matching is proposed to estimate relative motion in an Unscented Kalman Filter (UKF) framework.

Considering single-scan-based estimation [14]–[16] uses the information given by the observation angle and the radial velocity of multiple targets in a scan to instantaneously estimate linear and rotational velocities. Kellner et al. [17] presented this method using the Random Sample Consensus (RANSAC) algorithm for outlier rejection and Least

Titouan Tyack, Damien Vivet and Laurent Ferro-Famil are with ISAE-SUPAERO, University of Toulouse, Toulouse, France name.surname@isae-supaero.fr

This work was funded by AID, grant number 2022 65 0082

Squares(LSQ) to estimate the 2D twist that is integrated to get the 2D motion. Doer and Trommer [18] integrated this in an Error-State Extended Kalman Filter (ES-EKF) fusing 3D twist from the radar with Inertial Measurement Unit (IMU) data. Park et al. [19] presented a 3D pose graph multi-radar inertial odometry. Finally, in [20], Huang et al. proposed a factor graph-based multi-radar inertial 3D odometry.

Some solutions combining both techniques have also been studied. In [21], Zhuang et al. proposed a 4D radar inertial odometry and mapping solution based on an iterative Extended Kalman Filter which fuses ego-velocity estimation and scan-to-submap matching for state update. In [12], the ego velocity estimation is used to remove dynamic objects to use pre-processed scans during the matching part. In [13], the 2D velocity estimation is used to rectify the translation of sampled scans to improve matching performance.

Finally, in [22], Kubelka et al. propose a comprehensive study questioning the need for scan-matching versus single-scan estimation in radar odometry. The conclusion is that it depends highly on the radar used (radial velocity accuracy), on the scenario (parking, mine or forest) and the computational capabilities of the used system. The single-scan estimation will rely only on angle and radial velocity information. It will use the radar like a proprioceptive sensor as it is estimating an ego-motion by integrating an estimated velocity. Therefore, the accuracy is dependent on the accuracy of the radial velocity and the estimated pose will necessarily drift over time. On the other hand, scan matching based methods uses range and angle information. Its operability depends on the ability of the sensor to track targets over scans to estimate radar's relative transformation. If loop-closure is implemented [12], [21], it can remove the drifting issue but it comes at the cost of increased computational complexity.

While many state-of-the-art solutions rely on IMU and the use of optimization for ego velocity estimation, our fully filter-based algorithm uses an Implicit Extended Kalman Filter to predict each target's radial velocities based on their angle of arrival and the vehicle states $[v, \omega]$ to estimate its 2D trajectory. We propose a robust matching- and tracking-free approach that does not rely on additional IMU sensors.

### B. Calibration

The calibration corresponds to the ability to estimate transformation parameters from one sensor to another one or the vehicle reference frame. In terms of radar calibration, several works were presented relying on the use of reflective corners that are convenient for data association through consecutive scans coming from one radar or between multiple sensors [23]–[25]. Recently, target-less methods have been presented, facilitating the calibration process. Doer et al. [26] included in their radar-inertial odometry an online estimation of the 3D extrinsic parameters of the radar. In [27], a 2D calibration of radar pairs is presented, it relies on batch optimization of the fusion of estimated velocities by each radar and estimates the translation up to the scale and the rotation between two radars. Recently, in [28] and [29], Chen et al. submitted a spatiotemporal 3D targetless calibrator estimating the 3D extrinsic parameters between one or multiple exteroceptive sensors (camera, lidar, radar) and at least one IMU.

Whereas many of the calibration methods presented are based on an IMU, we propose in this paper a radar-only approach. Our approach consists of a multi-radar-vehicle calibration. It follows a two-step procedure with, first, an unknown 2D trajectory which allows estimating each radar's extrinsic angle. Secondly, a pure rotational motion where the knowledge of the baseline (inter-distance) between the two radars is needed to estimate the extrinsic translation as a sensor bench-vehicle calibration. Our solution is targetless, fully filter-based and dedicated to skid-steering vehicles.

## III. Radar Odometry ans State Estimation

### A. Observation model

In the case of mono radar navigation, a minimum of three static detections is needed to estimate the vehicle velocity [16]. As illustrated in figure 1, the radial velocity of the detected static targets (measured by the Doppler effect) corresponds to the projection of the radar velocity $\mathbf{V}^{S_i}$ in the direction of observation $\alpha_{ij}$. Thus, we can express the radial velocity $\hat{V}_{r,ij}$ associated with detection $j$ obtained by radar $i$ observed in the direction $\alpha_{ij}$ (see equation 1).

$$\hat{V}_{r,ij} = \mathbf{V}^{S_i,T} \begin{bmatrix} \cos\alpha_{ij} \\ \sin\alpha_{ij} \end{bmatrix} \tag{1}$$

From multiple observations, the optimal radar speed $\mathbf{V}^{\mathbf{S}*}$ can be obtained by least squares minimisation as shown in Equation 2. Note that an additional step to deal with outliers (potential moving objects or wrong detection) is required. One can use outlier rejection using RanSaC [17], [18], or by performing a weighted least square [16].

$$\left(\mathbf{V}^{\mathbf{S_i}*}\right) = \underset{(\mathbf{V}^{\mathbf{S_i}})}{\arg\min} \left( \sum_j (V_{r,ij} - \hat{V}_{r,ij})^2 \right) \tag{2}$$

By knowing the pose of the radar in the vehicle frame, the radar's velocity $\mathbf{V}^{S_i}$ is provided by the equation 3.

$$\mathbf{V}_i^{S_i} = \mathbf{R}_R^{S_i}(\beta_i) \left( \mathbf{V}_l^R + \begin{bmatrix} 0 \\ 0 \\ \omega_z^R \end{bmatrix} \times \begin{bmatrix} l_{x,i} \\ l_{y,i} \\ 0 \end{bmatrix} \right), \tag{3}$$

An Ackermann or a skid-steering vehicle, admits no sideslip meaning a null lateral velocity ($V_y^R = 0$). Thus, from (1) and (3) we can write the measurement model linking the state of the vehicle with the observed radial velocities as:

$$\begin{aligned} \hat{V}_{r,ij} &= (v_x^R - \omega_z^R l_{y,i})\cos(\beta_i + \alpha_{ij}) + \omega_z^R l_{x,i}\sin(\beta_i + \alpha_{ij}) \\ &= (v_x^R - \omega_z^R l_{y,i})\cos(\phi_{i,j}) + \omega_z^R l_{x,i}\sin(\phi_{i,j}) \end{aligned} \tag{4}$$

with $v_x^R$ and $\omega_z^R$ the linear and rotational velocities of the vehicle and $[l_x, l_y, \beta]$ the radar's extrinsic parameter.

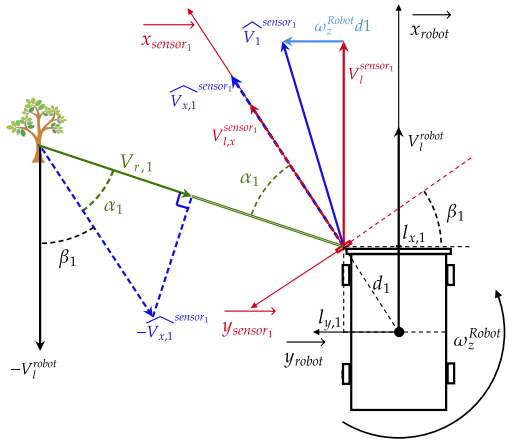


Fig. 1: Frame convention - in black robot frame, in red sensor frame

### B. State Estimation

The proposed radar-odometry consists of estimating the state of the vehicle from single or multiple radar sensors. For such applications, an Implicit Extended Kalman Filter (IEKF) has been employed in which the state of the vehicle and the extrinsic calibration of the system is estimated. In the next section, the state and measurement models used in the IEKF are described. Then the calibration process will be presented.

*1) Odometry:*

*State Model:* The state of the system is composed of the 2D pose of the vehicle $[x, y, \theta]$ and its linear and angular velocities $[v, \omega]$. The global state at time $k$ related to the vehicle to be estimated is then:

$$x_k = [x, y, \theta, v, \omega]^T$$

The behaviour of the system is supposed to be modelled by a Constant Velocity and Turning Rate (CTRV) model.

*Measurement Model:* As explained in the section III, the radial velocity of each target can be estimated from its angle of arrival (eq .1). It can be clearly seen that the radial velocity calculation is dependent on the angle of observation. Such formulation of the observation model is implicit (some observations are dependent on other observations). We then use classical IEKF equations in order to compute the innovation and its associated covariance according to equation 5:

$$\begin{aligned} \tilde{\boldsymbol{y}}_k &= \mathbf{V}_{\mathbf{r},k} - h\left(\hat{\boldsymbol{x}}_{k|k-1}, \boldsymbol{\alpha}_k\right) = \mathbf{V}_{\mathbf{r},k} - \hat{\mathbf{V}}_{\mathbf{r,k}} \\ \boldsymbol{S}_k &= \boldsymbol{H}_{\boldsymbol{x},k} \boldsymbol{P}_{k|k-1} \boldsymbol{H}_{\boldsymbol{x},k}^T + \boldsymbol{R}_{V_r,k} + \boldsymbol{H}_{\boldsymbol{\alpha}k} \boldsymbol{R}_{\alpha,k} \boldsymbol{H}_{\boldsymbol{\alpha}k}^T \end{aligned} \tag{5}$$

with the observation function $h$ given by equation 4 and $H_\alpha$ and $H_x$ are respectively the Jacobians of this $h$ function relative to the angle of arrival and the vehicle state.

*2) Odometry With Autocalibration:* The observation function 1 requires the knowledge of the extrinsic calibrations of the radars: $\beta_i$ the sensor orientation and $[l_x^i, l_y^i]$ the position of the sensor $i$ in the vehicle frame.

One of the solutions would be to estimate online the calibration parameters and to consider an enlarged state vector such as:

$$x_k = [x, y, \theta, v, \omega, C_1 \dots C_n]^T$$

with $C_i = [l_{x,i}, l_{y,i}, \beta_i]$ the extrinsic calibration (position and orientation) of the radar $i$ in the vehicle frame.

Nevertheless, a full online radar-vehicle calibration is not possible as $H_O$ the Jacobian of the measurement model with respect to the considered observables, given in equation 6, is rank deficient. The linear relations between the Jacobian columns is given in equation 7 and 8.

$$H_O = \begin{bmatrix} \frac{\partial \hat{\mathbf{V}}_{\mathbf{r},1}}{\partial v} & \frac{\partial \hat{\mathbf{V}}_{\mathbf{r},1}}{\partial \omega} & \frac{\partial \hat{\mathbf{V}}_{\mathbf{r},1}}{\partial C_1} & \dots & \mathbf{0} \\ \vdots & \vdots & \vdots & \ddots & \vdots \\ \frac{\partial \hat{\mathbf{V}}_{\mathbf{r},n}}{\partial v} & \frac{\partial \hat{\mathbf{V}}_{\mathbf{r},n}}{\partial \omega} & \mathbf{0} & \dots & \frac{\partial \hat{\mathbf{V}}_{\mathbf{r},n}}{\partial C_n} \end{bmatrix} \tag{6}$$

$$\begin{aligned} \frac{\partial \hat{\mathbf{V}}_{\mathbf{r,i}}}{\partial v} &= cos(\phi_\mathbf{i}) \\ \frac{\partial \hat{\mathbf{V}}_{\mathbf{r,i}}}{\partial \omega} &= -l_{y,i} cos(\phi_\mathbf{i}) + l_{x,i} sin(\phi_\mathbf{i}) \\ \frac{\partial \hat{\mathbf{V}}_{\mathbf{r,i}}}{\partial l_{x,i}} &= \omega sin(\phi_\mathbf{i}) \\ \frac{\partial \hat{\mathbf{V}}_{\mathbf{r,i}}}{\partial l_{y,i}} &= -\omega cos(\phi_\mathbf{i}) \\ \frac{\partial \hat{\mathbf{V}}_{\mathbf{r,i}}}{\partial \beta_i} &= -(v - \omega l_{y,i}) sin(\phi_\mathbf{i}) + \omega l_{x,i} cos(\phi_\mathbf{i}) \end{aligned}$$

$$\omega \frac{\partial \hat{\mathbf{V}}_\mathbf{r}}{\partial w} = \sum_i l_{x,i} \frac{\partial \hat{\mathbf{V}}_{\mathbf{r,i}}}{\partial l_{x,i}} + l_{y,i} \frac{\partial \hat{\mathbf{V}}_{\mathbf{r,i}}}{\partial l_{y,i}} \tag{7}$$

$$-\omega \frac{\partial h}{\partial v} = \sum_i \frac{\partial h}{\partial l_{y,i}} \tag{8}$$

Equations 7 and 8 mean that the influence of a variation on $v$, $\omega$ and $l_{x,i}$ $l_{y,i}$ are ambiguous and cannot be isolated. While the odometry can be performed in the mono- or multi-radar case, the calibration cannot be done considering only one radar. Indeed, using one radar, we cannot estimate simultaneously $v, \omega$ and $\beta$ due to the rank deficiency of the Jacobian of the measurement with respect to these observables. Therefore, we will consider the multi-radar-vehicle calibration problem. To solve it, we propose to realise the estimation in a two-step manner: first by estimating the sensors' orientations and then the sensors' positions.

*3) Estimation of sensors orientations:* Using at least two radars, the Jacobian of the observation model (eq. 4) wrt. $[v, \omega, \beta_1, ..., \beta_n]$ is of full column rank, which makes it possible to estimate the extrinsic angle of the radars even with a very poor a priori knowledge of their position.

*4) Estimation of the radars' lever-arms:* First, to leverage the rank deficiency due to (7), we propose to use two radars with a known inter-distance in a sensor bench configuration. By knowing the baseline $b = \sqrt{(l_{x,1} - l_{x,2})^2 + (l_{y,1} - l_{y,2})^2}$, we can add it as a measurement to our observation model, we then have $H_O$ as written in equation 9:

$$H_O = \begin{bmatrix} \frac{\partial \hat{\mathbf{V}}_\mathbf{r}}{\partial v} & \frac{\partial \hat{\mathbf{V}}_\mathbf{r}}{\partial \omega} & \frac{\partial \hat{\mathbf{V}}_\mathbf{r}}{\partial l_{x,1}} & \frac{\partial \hat{\mathbf{V}}_\mathbf{r}}{\partial l_{y,1}} & \frac{\partial \hat{\mathbf{V}}_\mathbf{r}}{\partial l_{x,2}} & \frac{\partial \hat{\mathbf{V}}_\mathbf{r}}{\partial l_{y,2}} \\ 0 & 0 & \frac{\partial b}{\partial l_{x,1}} & \frac{\partial b}{\partial l_{x,2}} & \frac{\partial b}{\partial l_{x,2}} & \frac{\partial b}{\partial l_{y,2}} \end{bmatrix} \tag{9}$$

Secondly, even with the described configuration, the equation 8 still remains true. Considering a pure rotational trajectory, we can remove $v$ from our estimation. As a result, we have the following state vector: $x_k = [\theta, \omega, l_{x,1}, l_{y,1}, l_{x,2}, l_{y,2}]$ with Jacobian of the measurement model with respect to $[\omega, l_{x,1}, l_{y,1}, l_{x,2}, l_{y,2}]$ which is now in full column rank.

## IV. Sensor Placement and Observability Analysis

### A. Principles

To mount two radar systems on a vehicle, it is of main concern to have a good sensor positioning. This is even more true for radars measuring Doppler which represents the apparent radial velocity.

To find the best sensor poses, the method presented in [16] is used. The observability of the state vector is evaluated thanks to the determinant of the information matrix which allows us to detect every non-observable configuration. The information matrix $\mathcal{I}$ can be computed with equation 10:

$$\begin{aligned}\mathcal{I} &= H_O^T R H_O \\ &= H_O^T (R_{V_r} + H_\alpha R_\alpha H_\alpha^T) H_O\end{aligned} \tag{10}$$

with $H_O, H_\alpha$ respectively the Jacobians of the measurement model concerning the considered observables and to the azimuth angle of each detection and $R_{V_r}, R_\alpha$ respectively the covariance matrices of the radial velocity and azimuth angle measurements.

### B. Experimental setup and results

To find the optimal sensor placement, we will compute $|\mathcal{I}|$, the determinant of the information matrix, for each possible radar pose. For this theoretical study, we consider that each radar admits detections that are uniformly distributed in their field of view (FOV) and that each radar is placed around the vehicle as depicted in figure 2. The mounting poses are indexed from 0 to 8. The vehicle is a skid-steering rover with length $L = 0.65m$ and width $W = 0.3m$, we based the measurements parameters on TI AWR1843 radar's specifications using $R_{V_r} = 0.02m/s$, $R_\alpha = 3\,\text{deg}$ [30] and $FOV_\alpha = \pm 50deg$ (based on 6dB-beamwidth). The results of observability analysis are shown in figure 3. Each plots are the results of the computation of $|\mathcal{I}|$ at each pose for one radar (a) and two radar (b,c,d). Plots (a,b) correspond to the observability of $[v, \omega]$ with the knowledge of the extrinsic calibration. In plot (c), the considered observables are $[v, \omega, \beta_1, \beta_2]$. Finally, plot (d), shows the observability in the zero velocity scenario estimating $[\omega, l_{x_1} l_{y_1}, l_{x_2}, l_{y_2}]$ having the knowledge of the baseline and the extrinsic angles. We computed $|\mathcal{I}|$ with several values of $\omega$ centered on 0 and kept the minimum value to take into account the vehicle's motion. For plots (a,b,c), we used $V_x = 1.5m/s$ and $\omega \in \{-0.3, 0, 0.3\}$ and the same (d) except $\omega = 0$.

In plot (d), since a lot of cells are equal to zero and that the accuracy of calibration has an impact on the accuracy of motion estimation, we propose a final metric for observability which corresponds to the element-wise multiplication of plot (b), (c) and (d). By doing this, we will first avoid the configurations where calibration cannot be performed and find the sensor placement that provides the optimal trade-off between motion estimation and calibration. The result of this metric is given in figure 4 and the resulting optimal sensor placements pairs are depicted in figure 5.

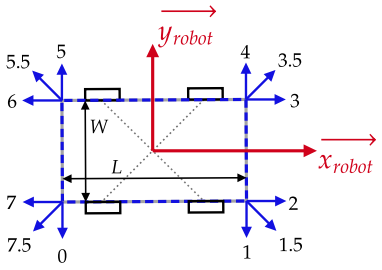


Fig. 2: Mounting poses indexing

### C. Sensor Placement results

These results can mainly be explained by two factors: the lever arm and the angle of observation: First, the bigger the lever arm, the better the observability. Second, in the multi-radar case, to maximize the observability, it is necessary to diversify the angle of observation. In the mono-radar case, if $\omega$ is positive, the optimal placement poses are 2 or 7, while if it is negative, the poses are 3 or 6, so the central poses that are 2.5 and 6.5 appears as a trade-off. In the mono radar case, the angle of observation is a trade-off , while in the multi radar case, we need to diversify the angle of observation of each radar.

An interesting point that justify the use of the proposed metric, is that the global maxima poses of observability of the velocity estimation (plot b), corresponds to global minima of the orientation estimation (plot c). The resulting optimal sensor placement in figure 4 correspond to local (plots b and d) or global (plot c) maxima in each scenarios. Finally, it is important to take into account that these results are highly dependent on the used parameter, i.e. the angle and radial velocity accuracies, the FOVs and the size of the vehicle.

## V. Odometry and Calibration Results

Simulations were conducted using Matlab Driving Scenario to create a realistic environment and a 120-meter trajectory. We used same parameters as presented in section IV-B, with a radar frequency of 10Hz. Extensive research on ego-motion velocity estimation based odometry has been carried out via simulations [18], [31]. The performance is influenced by the number, quality, and proportion of static versus moving targets, as well as sensor settings and trajectory parameter. In this study, we focus on the calibration process and its effect on odometry accuracy. We present first the calibration evaluation in the optimal sensor placement configuration. Then, we compare the odometry accuracy using the ground-truth calibration and with our estimated calibration.

### A. Radar sensor Calibration Simulation

The proposed experimentation of the calibration consists first by doing an unknown trajectory with noised extrinsic parameters on the lever-arm : $\sigma_{l_{x,y}} = 0.2m$, and on the extrinsic angles $\beta$ with two different level of noise: $\sigma_{high} = 20\,\text{deg}$ and $\sigma_{low} = 5\,\text{deg}$ and estimate the orientation of both radars. Then, to calibrate the lever-arm of the radars w.r.t the vehicle reference frame, for this second step we use

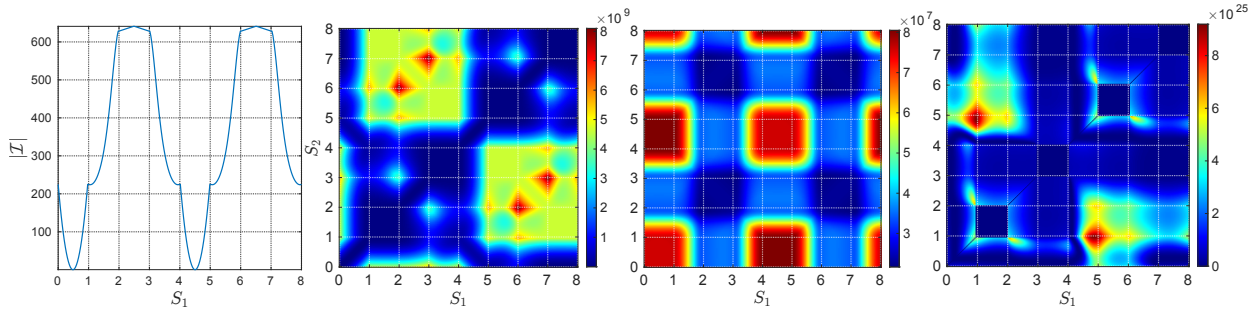


Fig. 3: Values of $|\mathcal{I}|$ are depicted on y-axis of plot (a) and with color on others. x-axis represents poses of sensor 1. On plots (b),(c) and (d) poses of sensor 2 are on y-axis. Plots (a) and (b) corresponds to velocity estimation for mono- and multi-radar. Plots (c) and (d) represents respectively the observability of orientation and lever-arm estimation.

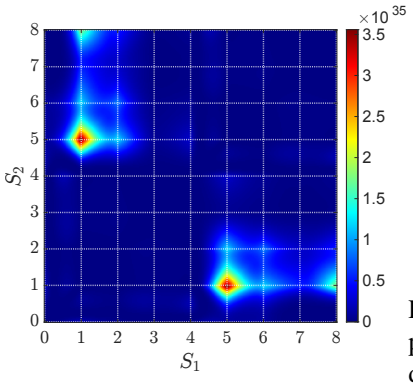

Fig. 4: Minimums of observability by element-wise multiplication

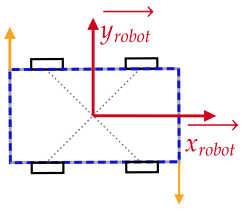


Fig. 5: Optimal sensor placements poses pair depicted in orange

the estimated radars orientations and the same noise on the radars' positions, and we perform a pure rotational trajectory. We performed 100 runs to compute Root-Mean Square Error (RMSE) of the estimated variables. The results obtained are depicted in the following table:

| | Orientation | Position |
|---|---|---|
| | $[\beta_1, \beta_2](deg)$ | $[l_{x,1} l_{y,1}, l_{x,2}, l_{y,2}](m)$ |
| RMSE $\sigma_{high}$ | $[2.26, 2.33]$ | $[9.4, 14.4, 9.5, 14.3] \times 10^{-3}$ |
| RMSE $\sigma_{low}$ | $[1.38, 1.12]$ | $[8.5, 9.2, 7.8, 7.7] \times 10^{-3}$ |

Note that in both noise case, we obtain a calibration accuracy that is better than the direction of arrival accuracy of the sensor ( $< 3\,\mathrm{deg}$) even considering a poor initial lever-arm knowledge. Considering the positioning of the sensor, the precision is in millimeter.

### B. Application to Odometry Simulation

We will present the odometry results first using the ground truth calibration and then using the estimated calibration. We computed Relative Pose Error (RPE) and Absolute Pose Error (APE) between the ground truth poses and the one estimated by the odometry in both cases. For the odometry with estimated calibration, we performed 100 runs with a noise level on the extrinsic parameters corresponding to the RMSEs detailed previously, therefore, the results are the mean RPE and APE over 100 runs.

| Odom | w/ GT calib | w/ est. calib $\sigma_h$ | w/ est. calib $\sigma_l$ |
|---|---|---|---|
| | $trans(m), rot(deg)$ | $t(m), r(deg)$ | $t(m), r(deg)$ |
| RPE | $[1.08, 0.15] \times 10^{-2}$ | $[0.23, 0.31]$ | $[0.21, 0.31]$ |
| APE | $[1.08, 0.07]$ | $[12.11, 16.37]$ | $[7.31, 16.7]$ |

In simulation, the odometry and the proposed calibration have shown promising results considering both the noise level on the extrinsic parameters and the accuracy of the radar used. Also, the low level of motion excitation has an impact on its quality.

### C. Calibration Using Real Data

Following the same protocol used previously in simulation, we tested the calibration with two radars, a TI AWR1843 and a TI AWR1843AOP, both mounted on a rover. The sensors were running at 20Hz. The configurations used for both radars correspond to $\alpha_{res,1843} = 15\,\mathrm{deg}, \alpha_{res,1843AOP} = 30\,\mathrm{deg}, Vr_{res} = 0.08m/s$. For the update, the measurement noise is based on the theoretical resolution of the sensor and the Signal to Noise Ratio (SNR) of the target, using $\sigma_x = x_{res}/\sqrt{SNR}$ with $x \in \{\alpha, Vr\}$. The radar mounting poses correspond to the configuration $[2, 5]$ shown in figure 2. The a priori calibration has been set, for the extrinsic angle estimation, to $C_1 = C_2 = [0, 0, 0]$, and for the position estimation, to $[l_x, l_y]_1 = [0.1, -0.1]$ and $[l_x, l_y]_2 = [-0.1, 0.1]$. The initial standard deviation of the calibration was defined as $10\,\mathrm{deg}$ and $0.1m$ for the angle and position. The outlier rejection used consists in a $\chi^2$ test on the Mahalanobis distance associated to each target. The results of the angle and position calibration are depicted in figure 6 and 7 respectively. We can see that the estimation of extrinsic parameters converges rapidly to relevant values considering the mounting poses. We ran angle calibration on several datasets and it always converged around these angles. The translation estimate depends on the defined baseline, but also converges to positions in line with the configuration. The final calibration values are $C_1 = [0.37, -0.17, 0.087]$ and $C_2 = [-0.34, 0.15, 1.503]$.

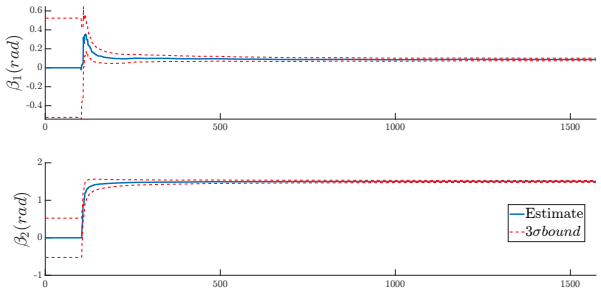


Fig. 6: Estimated extrinsic angles

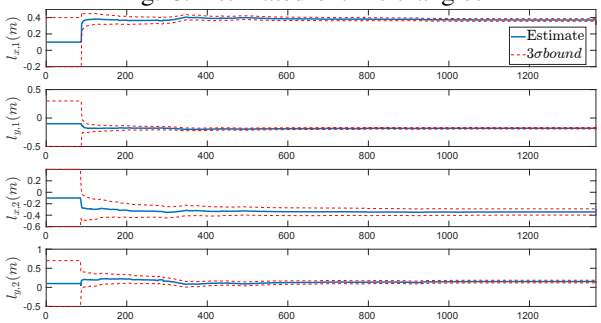


Fig. 7: Estimated extrinsic positions

## VI. Conclusion

This paper presented both a radar odometry and a calibration algorithms. First, we detailed our mono- or multi-radar odometry using an Implicit Extended Kalman Filter based on ego velocity estimation principles. Then, we proposed a filter-based, target-less multi-radar-vehicle extrinsic calibration algorithm. We suggested an observability analysis used to determine a trade-off sensor placement. Then, we detailed the simulations done on both odometry and calibration algorithms showing that the system calibrates itself and achieves good localization performances. Lastly, we gave some first results on the calibration estimation. In future works, we would like to use the range information provided by the radar to leverage the need of an a priori knowledge on the baseline and skid-steering hypothesis.

## References


[1] F. Feriol, D. Vivet, and Y. Watanabe, "A review of environmental context detection for navigation based on multiple sensors," *Sensors*.

[2] C. Campos, R. Elvira, J. J. G. Rodríguez, J. M. M. Montiel, and J. D. Tardós, "Orb-slam3: An accurate open-source library for visual, visual–inertial, and multimap slam," *IEEE Transactions on Robotics*, vol. 37, no. 6, pp. 1874–1890, 2021.

[3] T. Shan, B. Englot, D. Meyers, W. Wang, C. Ratti, and D. Rus, "Lio-sam: Tightly-coupled lidar inertial odometry via smoothing and mapping," in *2020 IEEE/RSJ International Conference on Intelligent Robots and Systems (IROS)*, 2020, pp. 5135–5142.

[4] Y. Zhou, L. Liu, H. Zhao, M. López-Benítez, L. Yu, and Y. Yue, "Towards deep radar perception for autonomous driving: Datasets, methods, and challenges," *Sensors*, vol. 22, no. 11, 2022.

[5] R. Weston, M. Gadd, D. De Martini, P. Newman, and I. Posner, "FastMbyM: Leveraging Translational Invariance of the Fourier Transform for Efficient and Accurate Radar Odometry," 2022.

[6] P. Furgale, J. Rehder, and R. Siegwart, "Unified temporal and spatial calibration for multi-sensor systems," in *2013 IEEE/RSJ International Conference on Intelligent Robots and Systems*, 2013, pp. 1280–1286.

[7] K. Koide, S. Oishi, M. Yokozuka, and A. Banno, "General, single-shot, target-less, and automatic lidar-camera extrinsic calibration toolbox," in *2023 IEEE International Conference on Robotics and Automation*.

[8] S. Mishra, G. Pandey, and S. Saripalli, "Target-free extrinsic calibration of a 3d-lidar and an imu," in *2021 IEEE International Conference on Multisensor Fusion and Integration for Intelligent Systems (MFI)*.

[9] T. Grebner, R. Riekenbrauck, and C. Waldschmidt, "Simultaneous Localization and Mapping (SLAM) for Synthetic Aperture Radar (SAR) Processing in the Field of Autonomous Driving," *IEEE Transactions on Radar Systems*, vol. 2, pp. 47–66, 2024.

[10] M. Steiner, T. Grebner, and C. Waldschmidt, "Millimeter-wave sar-imaging with radar networks based on radar self-localization," *IEEE Transactions on Microwave Theory and Techniques*, 2020.

[11] M. Holder, S. Hellwig, and H. Winner, "Real-time pose graph slam based on radar," in *2019 IEEE Intelligent Vehicles Symposium (IV)*.

[12] J. Zhang, H. Zhuge, Z. Wu, G. Peng, M. Wen, Y. Liu, and D. Wang, "4DRadarSLAM: A 4D Imaging Radar SLAM System for Large-scale Environments based on Pose Graph Optimization," in *2023 IEEE International Conference on Robotics and Automation (ICRA)*.

[13] H. Kim, H. Jang, and A. Kim, "2D Ego-Motion with Yaw Estimation using Only mmWave Radars via Two-Way weighted ICP," 2024.

[14] Y. Almalioglu, M. Turan, C. X. Lu, N. Trigoni, and A. Markham, "Milli-RIO: Ego-motion estimation with low-cost millimetre-wave radar," *IEEE Sensors Journal*, vol. 21, no. 3, pp. 3314–3323, 2021.

[15] S. Zhu, F. Fioranelli, and A. Yarovoy, "Radar-only instantaneous ego-motion estimation using neural networks," in *2023 20th European Radar Conference (EuRAD)*, 2023, pp. 201–204.

[16] A. Corominas-Murtra, J. Vallvé, J. Solà, I. Flores, and J. Andrade-Cetto, "Observability analysis and optimal sensor placement in stereo radar odometry," in *2016 IEEE International Conference on Robotics and Automation (ICRA)*, 2016, pp. 3161–3166.

[17] D. Kellner, M. Barjenbruch, J. Klappstein, J. Dickmann, and K. Dietmayer, "Instantaneous ego-motion estimation using multiple doppler radars," in *2014 IEEE International Conference on Robotics and Automation (ICRA)*, 2014, pp. 1592–1597.

[18] C. Doer and G. F. Trommer, "An EKF based approach to radar inertial odometry," in *2020 IEEE International Conference on Multisensor Fusion and Integration for Intelligent Systems (MFI)*, 2020.

[19] Y. S. Park, Y.-S. Shin, J. Kim, and A. Kim, "3D ego-Motion Estimation Using low-Cost mmWave Radars via Radar Velocity Factor for Pose-Graph SLAM," *IEEE Robotics and Automation Letters*, pp. 7691–7698.

[20] J.-T. Huang, R. Xu, A. Hinduja, and M. Kaess, "Multi-radar inertial odometry for 3d state estimation using mmwave imaging radar," 2024.

[21] Y. Zhuang, B. Wang, J. Huai, and M. Li, "4d iriom: 4d imaging radar inertial odometry and mapping," *IEEE Robotics and Automation Letters*, vol. 8, no. 6, pp. 3246–3253, 2023.

[22] V. Kubelka, E. Fritz, and M. Magnusson, "Do we need scan-matching in radar odometry?"

[23] B. Ubezio, H. Zangl, and M. Hofbaur, "Extrinsic Calibration of a Multiple Radar System for Proximity Perception in Robotics," in *2023 IEEE International Instrumentation and Measurement Technology Conference (I2MTC)*, 2023, pp. 1–6.

[24] E. Wise, Q. Cheng, and J. Kelly, "Spatiotemporal Calibration of 3-D Millimetre-Wavelength Radar-Camera Pairs," *IEEE Transactions on Robotics*, vol. 39, no. 6, pp. 4552–4566, 2023.

[25] T. Grebner, M. Linder, N. Kern, P. Schoeder, and C. Waldschmidt, "6D Self-Calibration of the Position and Orientation of Radar Sensors in a Radar Network," in *2022 19th European Radar Conference (EuRAD)*.

[26] C. Doer and G. F. Trommer, "Radar inertial odometry with online calibration," in *2020 European Navigation Conference (ENC)*.

[27] Q. Cheng, E. Wise, and J. Kelly, "Extrinsic Calibration of 2D Millimetre-Wavelength Radar Pairs Using Ego-Velocity Estimates," in *2023 IEEE/ASME International Conference on Advanced Intelligent Mechatronics (AIM)*, 2023, pp. 559–565.

[28] S. Chen, X. Li, S. Li, Y. Zhou, and S. Wang, "Ris-calib: An open-source spatiotemporal calibrator for multiple 3d radars and imus based on continuous-time estimation," 2024.

[29] S. Chen, X. Li, S. Li, Y. Zhou, and X. Yang, "iKalibr: Unified Targetless Spatiotemporal Calibration for Resilient Integrated Inertial Systems," 2024.

[30] H. A. Dell, "Introduction to radar systems. merrill i. skolnik. mcgraw-hill book co., london and new york. 1962." *The Journal of the Royal Aeronautical Society*, vol. 67, pp. 313 – 313, 1963.

[31] D. Kellner, M. Barjenbruch, J. Klappstein, J. Dickmann, and K. Dietmayer, "Instantaneous ego-motion estimation using doppler radar," in *16th International IEEE Conference on Intelligent Transportation Systems (ITSC 2013)*, 2013, pp. 869–874.